Heterogeneous & Homogeneous & Bio- & Nano-
CHEMCATCHEM
CATALYSIS

Accepted Article

Title: Pd Nanoparticles Encapsulated in FER Zeolite through Layer Reassembling Strategy as the Shape-selective Hydrogenation Catalyst

Authors: Zhenchao Zhao, Yanlu Li, Mathias Feyen, Robert McGuire, Ulrich Müller, and Weiping Zhang

To be cited as: *ChemCatChem* 10.1002/cctc.201800040

Link to VoR: http://dx.doi.org/10.1002/cctc.201800040

A Journal of
ChemPubSoc Europe

WILEY-VCH

www.chemcatchem.org

10.1002/cctc.201800040

Pd Nanoparticles Encapsulated in FER Zeolite through Layer Reassembling Strategy as the Shape-selective Hydrogenation Catalyst

Zhenchao Zhao,[a] Yanlu Li,[a] Mathias Feyen,[b] Robert McGuire,[b] Ulrich Müller,*[b] and Weiping Zhang*[a]

[a] *State Key Laboratory of Fine Chemicals, School of Chemical Engineering, Dalian University of Technology, Dalian 116024, China*

[b] *BASF SE, Process Research and Chemical Engineering, 67056 Ludwigshafen, Germany*

*Corresponding authors. E-mail:ulrich.mueller@basf.com (U. Müller), wpzhang@dlut.edu.cn (W. Zhang)

Abstract: Noble metal nanoparticles (NPs) encapsulated in zeolites bearing distinct shape-selective properties at molecular level expand their new applications in catalysis. Here we report a synthesis strategy for the encapsulation of Pd NPs inside FER zeolite via alayer reassembling process. Pd precursors were introduced by swelling FER layers in RUB-36 through the surfactant cetyltrimethylammonium cations (CTA^+) and then the ion-exchange process at ambient temperature. Pd@FER was formed with a uniform diameter distribution of Pd NPs at about 1.4 nm during the topotactic transformation from layered zeolite precursors to 3-dimensional zeolites followed by calcination. The as-prepared Pd@FER catalyst exhibits distinct shape-selective properties in hydrogenation reactions. It has relatively lower activity for 1-hexene and almost no activity for 1-phenyl-1-cyclohexene compared with Pd/RUB-37 catalyst prepared via wet impregnation due to the restrictions of channels in FER zeolite. On the contrary, Pd@FER shows very high hydrogenation activity for benzaldehyde and very low activity for diphenylmethanone hydrogenation, while Pd/RUB-37 exhibits high hydrogenation activity for both benzaldehyde and diphenylmethanone. This synthesis strategy may be extended in other noble metals or two-dimensional layered zeolite systems for size-selective hydrogenation reactions.

Keywords: Pd nanoparticles; FER zeolite; Layered zeolite; Layer reassembly; Shape-selective hydrogenation catalyst

1. Introduction

Metal nanoparticles (NPs) in zeolites are very intriguing catalysts as their distinct selectivity and activity for various types of catalytic reactions.[1] Therefore, a variety of approaches have been developed to prepare the metal NPs in zeolites. For large-pore zeolites with 12-membered ring (MR) structures such as FAU, MOR, LTL, BEA, AFI, etc., encapsulation of metal NPs in the cages or channels has been generally achieved by introducing metal precursors after zeolite crystallization using ion-exchange, impregnation, or chemical vapor deposition.[1a, 2] For smaller-pore zeolites with 10 or 8-MR structures, above mentioned methods are not so efficient as the smaller apertures. This problem has been well addressed by introducing metal precursors or NPs during zeolite crystallization process, and the metal precursors or NPs were embedded in the zeolite crystals during their crystallization.[1b, 3] Metal NPs such as Ni, Au, Ag, Pt, Pd, Ru, and Rh were introduced in MFI, SOD, BEA, FAU zeolites using metal complex or synthesized NPs during crystallization of zeolite.[1b, 3a-e, 4] Although so many elegant methods have been developed, the efficient introduction of metal NPs is still challenging. Charge densities, pore sizes of zeolites and stability/size of the metal precursor have great impacts on the efficiency of encapsulation. For ion-exchange method, the amount of metal introduced in zeolite matrix is strongly dependent on the Si/Al ratios, which determines the available ion-exchange sites. Whereas, introduction of metal precursors during the hydrothermal synthesis of zeolite requires the metal precursors has high hydrothermal stability under alkaline condition.

Moreover, most of above investigations are focused on the 3-dimensional framework zeolites. Some zeolites such as MCM-22, Ferrierite, Sodalite, RUB-24, CDS-1(RUB-37), RUB-41, etc. can be obtained from their layered precursors (LPS) MCM-22P, PREFER, RUB-15, RUB-18, PLS-1(RUB-36), RUB-39, respectively.[5] These LPS with flexible layer distance, which may be very good candidates for the introduction of the guest metal precursors/NPs.[6] The expansion of layer distance makes the layers accessible for most metal precursors and even metal NPs. Very recently, subnanometric Pt clusters with 0.11 wt% loading were prepared using dimethyl formamide (DMF) as a weak reduction and capping agent during transformation of a 2D zeolite into 3D high silica MCM-22 zeolite.[7] Previous

investigations of ours[8] and other groups[9] demonstrate that the layered structure in LPS can be well preserved during the layer swelling and deswelling processes at room temperature, and after calcination the 3-dimensional zeolite structure maintains. In swollen LPS, a large amount of positively charged swelling agents balanced by negatively charged SiO^- groups provides very rich ion-exchange sites.[8, 10] Herein, we report a new synthesis strategy for FER zeolite encapsulating Pd NPs via a layer reassembling process with Pd precursors introduced at ambient temperature, which are proved to be very effective catalysts for the size-selective hydrogenation reactions.

2. Results and Discussion

2.1 Our synthesis strategy

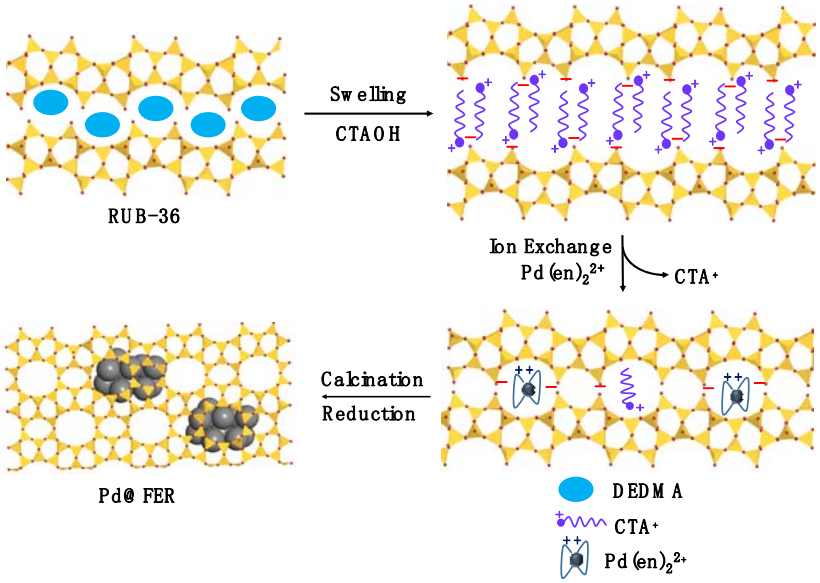

Scheme 1. Illustration showing encapsulation of Pd NPs in FER zeolite through layer reassembling strategy.

Scheme 1 illustrates the encapsulation process of Pd NPs in FER zeolite through layer reassembling strategy. Firstly, RUB-36 was swollen into RUB-36SW composed by negatively charged FER layers (SiO^-) and positively charged cetyltrimethylammonium cations(CTA^+), and the original organic template diethyldimethyl ammonium (DEDMA) was excluded. Then palladium precursor (Diethylenediamine palladium(II) acetate, $Pd(en)_2(Ac)_2$)

was introduced via ion-exchange of CTA^+ with $Pd(en)_2^{2+}$ in an ethanol solution at ambient temperature. Simultaneously, the distances between FER layers recover due to removal of most long chain CTA^+ with smaller $Pd(en)_2^{2+}$. After washing in deionized water, most $Pd(en)_2^{2+}$ outside of FER layer aggregate were removed due to regeneration of silanol groups under the neutral pH conditions. Finally, the formation of metal NPs and condensation of silanol groups between the adjacent FER layers was accomplished via 500 °C calcination and 350 °C reduction processes.

2.2 XRD and ^{13}C NMR characterizations

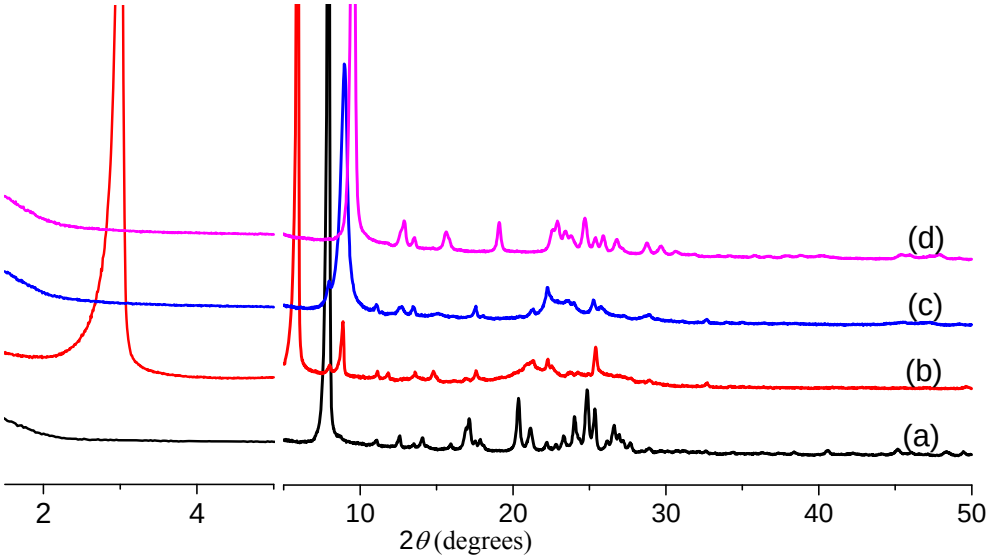

Figure 1. XRD patterns of (a) RUB-36; (b) swollen RUB-36; (c) deswelling material obtained by ion exchange with $Pd(en)_2^{2+}$ and En-HAc; (d) Pd@FER obtained after calcination and H_2 reduction.

The encapsulating process of Pd NPs in FER zeolite was followed by the XRD patterns as shown in Figure 1.Firstly, the distances between FER layers in RUB-36 were expanded from 11.2 Å (2θ= 7.9°) to 29.4 Å (2θ= 3.0°) after swelling (Figure 1a-b). This distance offering enough space allows $Pd(en)_2^{2+}$ to access to the FER layers. When $Pd(en)_2^{2+}$ was introduced (Figure 1c) in the presence of ethylenediamine-acetic acid (En-HAc), the low-angle diffractions of 2θ= 3.0° (100) and 2θ= 5.9° (200) diminish, and a new broad peak near 2θ = 9.0° appears, corresponding to FER layer distance of 9.7 Å. This is similar to our previously reported deswelling process using dilute acidic solution to exclude CTA^+.[8] Over

calcination in air and reduction with hydrogen, the obtained Pd@FER (Figure 1d) has the same diffraction pattern as FER zeolite with very good crystallinity.[11] Moreover, the absence of the diffractions of Pd metal crystals near 40° and 46° means that PdNPs are ultrafine without significant aggregated bulk ones. ICP-AES analysis shows that the Pd loading is 1.4 wt%.

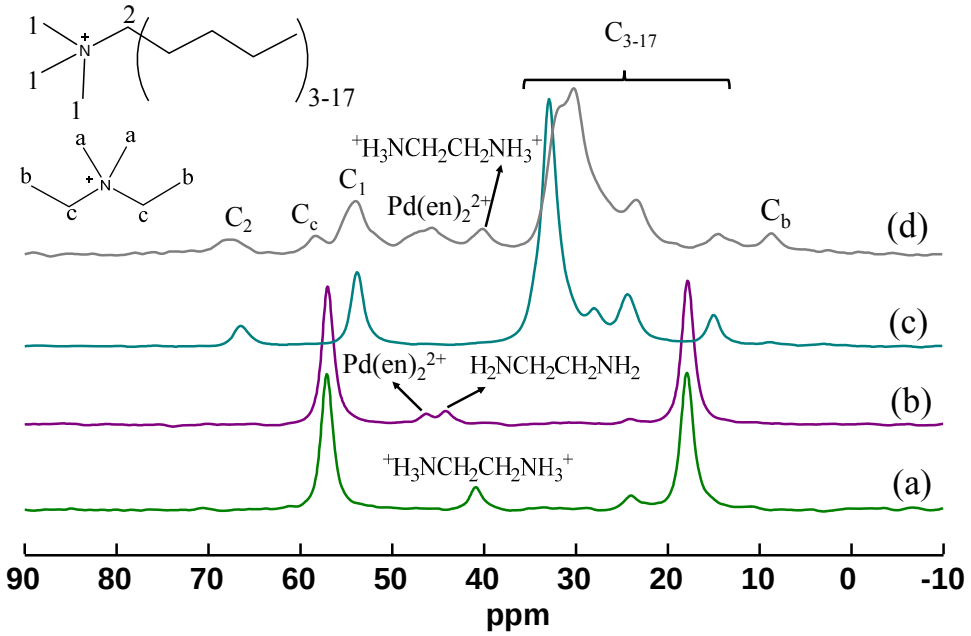

Figure 2. Solution ^{13}C NMR spectra of (a) ethylenediamine-acetic acid (En-HAc) solution in ethanol; (b) $Pd(en)_2(Ac)_2$ and En solution in ethanol. ^{13}C CP/MAS NMR spectra of RUB-36SW (c) and deswelling material obtained by ion exchange with $Pd(en)_2^{2+}$ (d) .

As very rich amount of terminalsilanol groups on the surface of each FER layer, the amount of Pd loadings could reach very high up to 13 wt%. It should be pointed out that a certain amount of En-HAc solution should be co-added with $Pd(en)_2^{2+}$ to obtain FER zeolite with high crystallinity. Even though $Pd(en)_2^{2+}$ can deswell RUB-36SW without En-HAc (Supporting Information, Figure S1a), too much amount of Pd may hinder the ordered condensation of silanol groups between the FER layers (Supporting Information, Figure S1b). ^{13}C CP/MAS NMR spectrum (Figure2c) of RUB-36SW indicates the signals are attributed to CTA^+. After deswelling, the remaining signals are still from the residual CTA^+ (Figure 2d), which may also act as the structure-directing agent for the ordered stacking of FER layers. Meanwhile, two new signals near 40 and 46 ppm are observed. According to the

solution ^{13}C NMR specra in Figures 2a-b, these signals can be assigned to pronated ethylenediamine and $Pd^{2+}(en)_2$.[12] It means that Pd precursors were successfully introduced between the FER layers. The minor remaining signals of DEDMA may result from very small amount of incompletely swollen RUB-36, which could be observed in XRD patterns (Figures 1b-c).

2.3 Nanostructure and Morphology Analysis

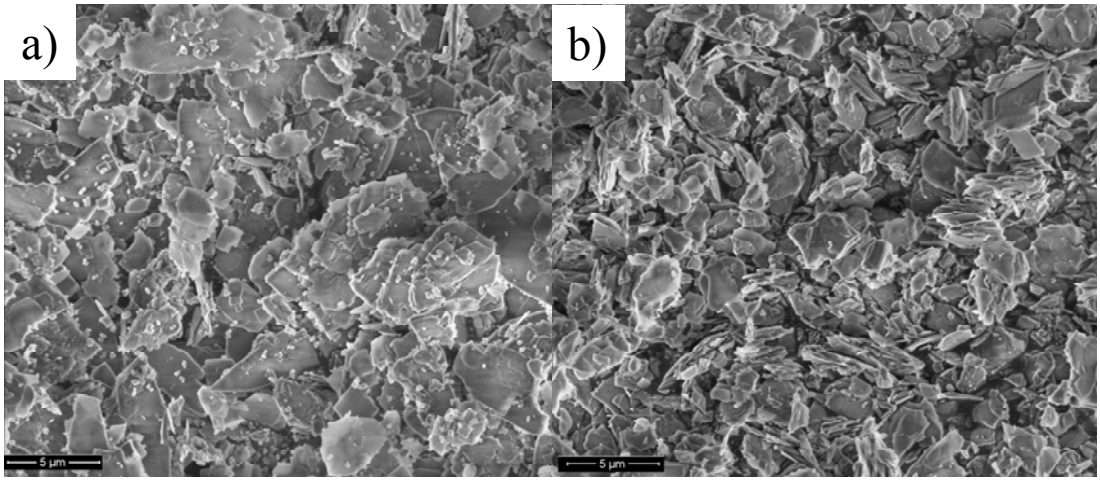

Figure 3. SEM images of Pd@FER (a) and Pd/RUB-37 (b).

SEM images in Figure3 demonstrate that Pd@FER has the typical flake morphologies similar to Pd/RUB-37 which was prepared by the incipient wetness impregnation using calcined RUB-36 i.e. RUB-37 as the support with 0.9 wt% Pd loading. It's worth noting that some debris on the FER zeolite (Figure 3a) may result from disaggregation of amorphous silica aggregate from RUB-36 during the alkaline swelling process.TEM and STEM images (Figure 4a-c) indicate ultrafine and well dispersed Pd NPs with an average particle size of 1.4 nm intensively distributed in the zeolite support, and only very minor bulk ones near the edge of zeolite sheet for Pd@FER (Figure 4a, red marks), which is reasonable due to the migration of Pd atoms between FER layers and further sintering near the edges during high temperature calcination. In comparison, Pd/RUB-37 (Figure 4e-g) shows Pd NPs with relatively broad size distributions dispersed on the supports with an average particle size of 4.2 nm. It's worth noting that the 1.4 nm size of Pd NPs embedded in FER zeolite is actually

much larger than the pore diameters of 5.4 × 4.2 Å and the side-cages (about 7 Å).[13] It can be explained by the fact that both the formation of 3D zeolite and Pd NPs occurrs during the calcination process, and once Pd NPs are formed larger than the pore size before the ordered condensation of silanol groups, the defects may be created. This is further confirmed by ^{29}Si MAS NMR spectrum of Pd@FER which shows significant amount of SiOH groups remaining on the support (Figure S2). It's also the case when too much $Pd(en)_2^{2+}$ was introduced between the FER layers, the ordered FER structure could not be obtained (Supporting Information, Figure S1). In comparison with Pd/RUB-37, even though the same metal precursor $Pd(en)_2(Ac)_2$ was used, the homogeneous distribution of Pd NPs with extremely high density within FER zeolite without significant sintering may result from its distinctive two-dimensional structure. Pd precursors or NPs are separated by the FER layers with no micropores, which hinders the particle sintering among different layers, and therefore enhance the thermal stability of Pd NPs.[14] N_2 adsorption/desorption isotherm of Pd@FER shows a typical Langmuir-type adsorption (Figure S3), indicating the presence of uniform micropores with a Brunauer-Emmett-Teller (BET) surface area of 325 m^2/g, which is close to that of 340 m^2/g for FER zeolite obtained by the similar topotactic conversion process.[8]

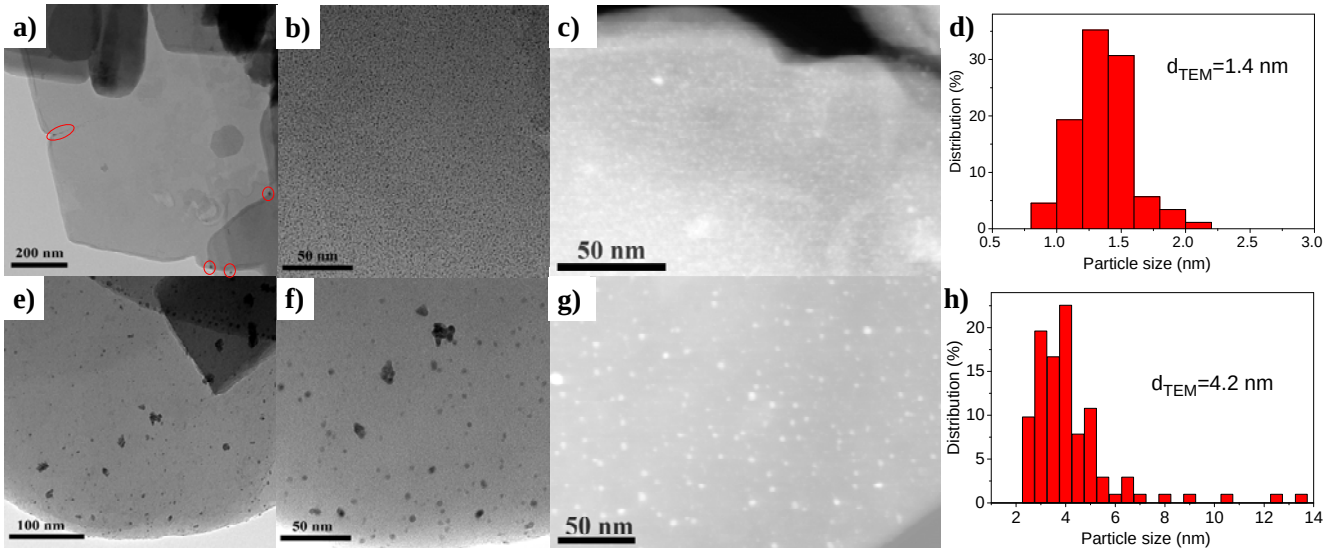

Figure 4. TEM (a,b,e,f), STEM (c,g) images and corresponding particle size distributions of Pd@FER (a,b,c,d) and Pd/RUB-37 (e,f,g,h) obtained after calcination and H_2 reduction.

10.1002/cctc.201800040

X-ray photoelectron spectroscopy (XPS) was also used to study the chemical state of Pd NPs with the spetra shown in Figure 5. Both samples show metallic Pd with 3d binding energies (BE) near 340.3 and 335.0 eV, respectively. [15] The signal intensity of Pd/RUB-37 is significantly stronger than that of Pd@FER, which is in accordance with the fact that most of Pd NPs are embeded between FER layers in FER zeolite while most of Pd NPs are located on the surface of RUB-37 zeolite.

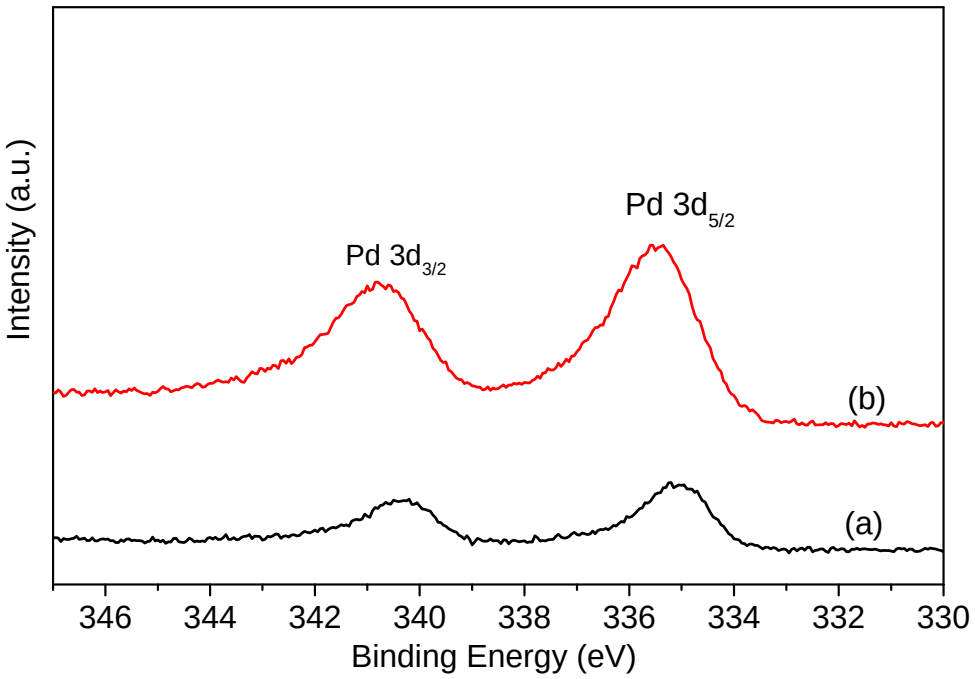

Figure 5. XPS spectra of Pd@FER (a) and Pd/RUB-37 (b).

2.4 Catalytic Hydrogenation Performances

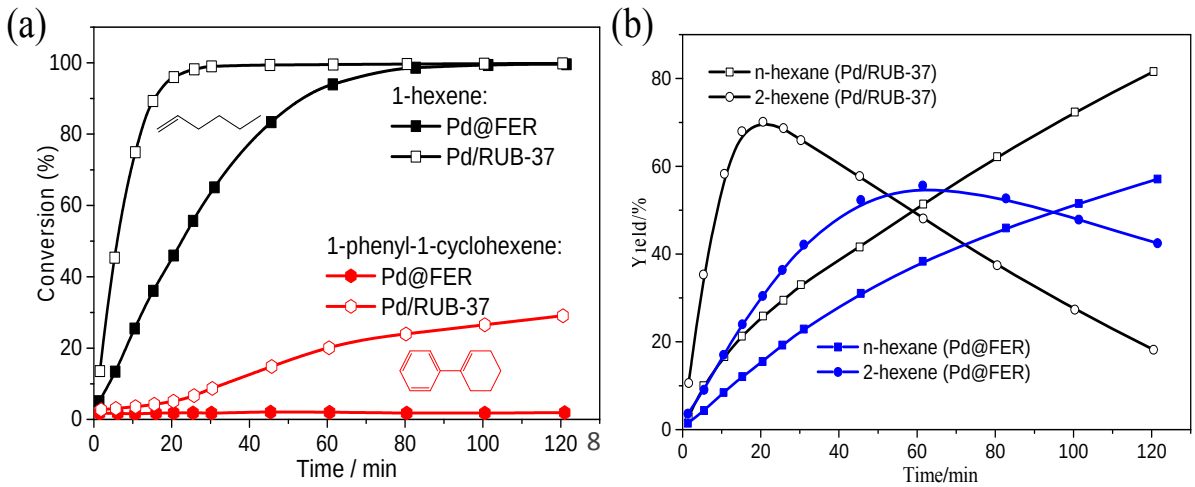

Figure 6. Hydrogenation activities of 1-hexene and 1-phenyl-1-cyclohexene (a), and time on stream product distributions for 1-hexene hydrogenation (b) over Pd@ZSM-35 and Pd/RUB-37 catalysts.

To further verify the successful encapsulation of Pd NPs in FER zeolite, model hydrogenation reaction of 1-hexene (4.3 Å), and 1-phenyl-1-cyclohexene with different steric hindrance were conducted. The reaction kinetic profiles of the olefin substrates and the product distributions are shown in Figure 6. As FER zeolite has apore size of 5.4 × 4.2 Å, 1-hexene has amolecular size close to the pore apertures shows relatively lower reaction rate for Pd@FER catalyst, and the 100% conversion of 1-hexene takes about 80 min(Figure 6a). Whereas, 100% conversion reaches for Pd/RUB-37 within 30 min. When 1-phenyl-1-cycohexene with much larger steric hindrance is used as substrate, there is almost no conversion for Pd@FER catalyst, while 30% 1-phenyl-1-cycohexene conversion is obtained for Pd/RUB-37 catalyst. It is worth noting that for 1-hexene hydrogentaion reaction, there is appreciable amount of isomerization product,2-hexene, for both catalysts (Figure 6b), and further transformation of 2-hexene is again significant slower for Pd@FER due to the steric hindrance.

Moreover, the selective C=O hydrogenation for benzaldehyde and diphenylmethanone were also tested and the reaction kinetic curves and the product distributions are shown in Figure 7. Pd@FER shows high hydrogenation activity for benzaldehyde, and the conversion of benzaldehyde reaches 100% within 100 min. While Pd/RUB-37 shows lower benzaldehyde conversion, it reaches about90% within 120 min (Figure 7a). Moreover, after reaction for 120 min Pd/RUB-37 catalyst has significant amount of intermediate hydrogenation product, benzylalcohol, and only 66% toluene yield is achieved (Figure 7b). Whilefor Pd@FER catalyst 100% toluene yield is obtained.On the contrary, for the much larger diphenylmethanone, Pd/RUB-37 show very high activity, and after 60 min diphenylmethanone is 100% transformed into diphenylmethane. No more than 10% of diphenylmethanoneis transformed after 120 min for Pd@FER due to the steric hindrance. Thislowdiphenylmethanone conversion may result from theminor bulk Pd NPs near the edge of the zeolite sheet (Figure 4a). All these results unambiguously demonstrate the shape-dependentselectivity of Pd@FER for hydrogenation reactions, and confirm the

successful encapsulation of most Pd NPs inside FER zeolite.

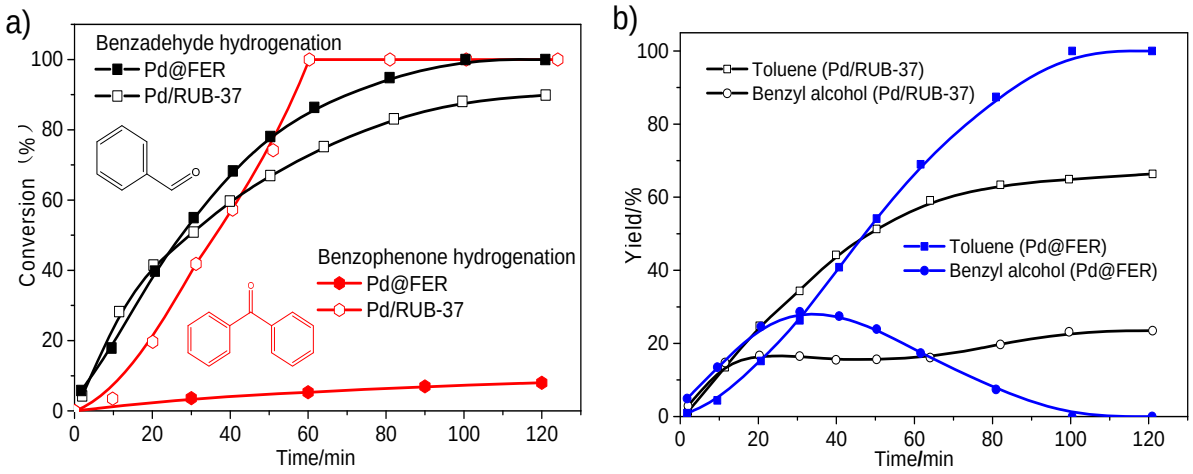

Figure 7. Hydrogenation activities of benzaldehyde and diphenylmethanone (a), and time on stream product distributions for benzaldehyde hydrogenation (b) over Pd@ZSM-35 and Pd/RUB-37 catalysts.

3. Conclusions

Pd@FER catalyst is successfully constructed via a new layer reassembling strategy. FER layers in RUB-36 were expaned via cetyltrimethylammonium cations (CTA^+) swelling. Subsequently, CTA^+ was exchanged by $Pd(en)_2^{2+}$, and $Pd(en)_2^{2+}$ was enclosed between FER layers. Pd NPs were embeded in FER zeolite during calcination when ordered condensation of silanol groups occurred between adjacent FER layers. Pd@FER was formed during the topotactic transformation from layered zeolite precursors to 3-dimensional zeolites during calcination. The as-synthesized Pd@FER shows excellent shape-selectivity in the hydrogenation of olefins, benzaldehyde and diphenylmethanone with different molecular sizes or steric hindrance due to its unique nanostructure and microporosity. Our synthetic strategy expands the scope of on-demand controlling the selectivity of metal nanoparticles by using two dimensional layered zeolite precursors with open structure.

Experimental Section

Sample preparation

The layered silicate RUB-36 was prepared similarly to our previous procedures using

diethyldimethylammonium hydroxide as the structure-directing agent (DEDMAOH, 20 wt% solution in water, Sachem Inc.).[8, 16] In general, it was crystallized from the gel with a composition of SiO_2 : 0.5 SDA : 10 H_2O. Aerosil 200 was utilized as the silica source. Crystallization was carried out in an autoclave without stirring for 14 days. The resultant product was filtered, washed with deionized water and dried at 100 °C.

Preparation of diethylenediamine palladium (II) acetate solution ($Pd(en)_2(Ac)_2$) and ethylenediamineacetic acid solution (en-HAc): 0.3 g palladium acetate (Aladdin Reagent) was dispersed into 9 ml ethanol containing 0.5 g ethylenediamine (Tianjin Bodi Chemical Co., Ltd.). After sonification for 10 min, a clear ethanol solution of $Pd(en)_2(Ac)_2$ was obtained. 1.0 g acetic acid (Tianjin Fuyu Fine Chemical Co., Ltd.) was dissolved into 9.0 ml ethanol containing 1.0 g ethylenediamine and 0.6 g deionized H_2O to get a clear solution of en-HAc.

RUB-36 was swollen by CTAOH (10 wt % solution in water, TCI) at room temperature (RT). Typically, 0.5 g RUB-36 was dispersed in the 35.0 g CTAOH solution (4 wt % solution in water). The mixture was stirred for 48 h, then filtered and washed with deionized water, and finally dried at RT. $Pd(en)_2Ac_2$deswelling process was conducted by mixing 0.5 g swollen sample with a mixture of 10 ml ethanol, 0.31 ml above prepared $Pd(en)_2Ac_2$ solution and 1.25 ml en-HAc solution, then stirred for 4 h at RT. The product was recovered by filtration, repeated washing with deionized water, ethanol and dried at RT. Calcination of obtained samples were conducted at 500 °C in static air for 4 h.

Pd/RUB-37 was prepared by incipient wetness impregnation method. Typically, 2.6 ml deionized H_2O was mixed with 0.2 ml en and 0.04 g $Pd(Ac)_2$ to get a clear aqueous solution of $Pd(en)_2Ac_2$. Then, above solution was dropwised into 2.0 g dried RUB-37. The sample was dried at RT and calcined at 500 °C in static air for 4 h. All the calcined samples were reduced at 350 °C under 30 ml/min 30% H_2/N_2 for 1 h.

Characterizations

XRD patterns were collected on the PANalytical X'Pert3 Powder X-ray diffractometer with Cu K_α radiation in the 2θ range of 0.5-10° and 5-50° and scan step size of 0.026°. Nitrogen adsorption/desorption measurements were carried out on a Micromeritics 2020

analyzer at 77 K after the samples were degassed at 350 °C under vacuum. X-ray photoelectron spectroscopy (XPS) measurements were performed on a Thermo Scientific ESCALAB 250Xi spectrometer using an Al Karadiation (15 kV, 10.8 mA, hυ = 1486.6 eV), calibrated internally by the carbon deposit C(1s) (E_b = 284.6 eV). Solution ^{13}C NMR, solid-state ^{13}C CP/MAS NMR and ^{29}Si MAS NMR were performed on an Agilent DD2-500 MHz spectrometer at 125.7 and 99.3 MHz, respectively. ^{13}C CP/MAS NMR spectra were collected using a 4 mm MAS NMR probe with a spinning rate of 8 kHz, a contact time of 2 ms and a recycle delay of 4 s. ^{29}Si MAS NMR spectrum was acquired using a 6 mm MAS NMR probe with as spinning rate of 4 kHz and a recycle delay of 30 s. Pd contents of the resulted catalysts were determined by Inductively Coupled Plasma Atomic Emission Spectroscopy (ICP-AES, Optima 2000 DV, USA). SEM and STEM images were obtained using a Hitachi S-5500 SEM equipped with a scanning transmission electron microscope (STEM), operating at an accelerating voltage of 30 kV. Transmission electron microscopy (TEM) images were recorded on Hitachi HT 7700 microscope operated at an acceleration voltage of 100 kV.

Catalytic hydrogenation tests

The catalytic activities of Pd@FER and Pd/RUB-37 were evaluated by hydrogenation reactions of 1-hexene (Aladdin Reagent), 1-phenyl-1-cyclohexene (Aladdin Reagent), benzaldehyde (Aladdin Reagent) and diphenylmethanone (Aladdin Reagent) with hydrogen. Typically, about 21 mg catalysts were loaded in a 50 ml stainless-steel autoclave equipped with a magnetic stirrer in a thermostat. After air in the reactor was purged with nitrogen, and the reactor was pressurized with hydrogen at 0.4 MPa and the catalysts were activated at 150 °C for 1 h. After cooling down to RT, 20 ml n-heptane (Beijing Chemical Reagent) were added, and the temperature was elevated to the desired one (40 °C for 1-hexene and 90 °C for 1-phenyl-1cyclohexene). Then 2 ml 1-hexene or 0.5 ml 1-phenyl-1-cyclohexene were added into the reactor. Immediately, 0.4 MPa H_2 were flushed in the reactor. Benzaldehyde and diphenylmethanone hydrogenation reactions were carried out at 80 °C similarly to above procedure. Specifically, 40 mg catalysts, 10 mmol benzaldehyde or 1 mmol diphenylmethanone were added in 30 ml n-heptane or ethanol, respectively. 0.1 ml samples

were taken out from the reactor at regular intervals, and the products were analyzed by a gas chromatography (Shimadzu GC-2014) equipped with a 30m HP-5 capillary column and flame ionization detector.

Acknowledgements

This work was financially supported by the National Natural Science Foundation of China (Nos. 21603022, 21673027), the Fundamental Research Funds for the Central Universities in China (Nos. DUT16RC(3)002, DUT17TD04), Open Project Funds of the State Key Laboratory of Catalysis, Dalian Institute of Chemical Physics (No.N-16-08) and the INCOE (International Network of Centers of Excellence) project coordinated by BASF SE, Germany.

Supporting Information

XRD patterns of only $Pd(en)_2Ac_2$deswollen RUB-36SW and calcined sample. ^{29}Si MAS NMR spectrum of Pd@FER. N_2 adsorption/desorption isotherms of Pd@FER and Pd/RUB-37.

References

[1] a) W. M. H. Sachtler, *Acc. Chem. Res.* **1993**, *26*, 383-387;b) N. Wang, Q. Sun, R. Bai, X. Li, G. Guo, J. Yu, *J. Am. Chem. Soc.* **2016**, *138*, 7484-7487.

[2] a) P. Gallezot, in *Post-Synthesis Modification I*, Springer Berlin Heidelberg, Berlin, Heidelberg, **2002**, pp. 257-305;b) M. Zahmakıran, Y. Tonbul, S. Özkar, *J. Am. Chem. Soc.* **2010**, *132*, 6541-6549.

[3] a) M. Choi, Z. Wu, E. Iglesia, *J. Am. Chem. Soc.* **2010**, *132*, 9129-9137;b) S. Goel, Z. Wu, S. I. Zones, E. Iglesia, *J. Am. Chem. Soc.* **2012**, *134*, 17688-17695;c) J. Gu, Z. Zhang, P. Hu, L. Ding, N. Xue, L. Peng, X. Guo, M. Lin, W. Ding, *ACS Catal.* **2015**, *5*, 6893-6901;d) T. L. Cui, W. Y. Ke, W. B. Zhang, H. H. Wang, X. H. Li, J. S. Chen, *Angew. Chem. Int. Ed.* **2016**, *55*, 9178-9182;e) C. Wang, L. Wang, J. Zhang, H. Wang, J. P. Lewis, F.-S. Xiao, *J. Am. Chem. Soc.* **2016**, *138*, 7880-7883;f) E. M. Barea, V. Fornes, A. Corma, P. Bourges, E. Guillon, V. F. Puntes, *Chem. Commun.* **2004**, 1974-1975.

[4] a) B.-Z. Zhan, M. A. White, T.-K. Sham, J. A. Pincock, R. J. Doucet, K. V. R. Rao, K. N. Robertson, T. S. Cameron, *J. Am. Chem. Soc.* **2003**, *125*, 2195-2199;b) J. Zhang, L. Wang, Y. Shao, Y. Wang, B. C. Gates, F.-S. Xiao, *Angew. Chem. Int. Ed.*, **2017**, *56*, 9747-9751;c) D. Wang, B. Ma, B. Wang, C. Zhao, P. Wu, *Chem. Commun.* **2015**, *51*, 15102-15105;d) C. Liu, J. Liu, S. Yang, C. Cao, W. Song, *ChemCatChem* **2016**, *8*, 1279-1282.

[5] a) B. Marler, H. Gies, *Eur. J. Mineral.* **2012**, *24*, 405-428;b) W. J. Roth, P. Nachtigall, R. E. Morris, J. Cejka, *Chem. Rev.* **2014**, *114*, 4807-4837;c) B. Yilmaz, U. Muller, B. Tijsebaert, D. D. Vos, B. Xie, F.-S. Xiao, H. Gies, W. Zhang, X. Bao, H. Imai, T. Tatsumi, *Chem. Commun.* **2011**, *47*, 1812-1814.

[6] Z. C. Zhao, W. P. Zhang, *Acta Phys.-Chim. Sin.* **2016**, *32*, 2475-2487.

[7] L. Liu, U. Diaz, R. Arenal, G. Agostini, P. Concepcion, A. Corma, *Nat Mater* **2017**, *16*, 132-138.

[8] Z. Zhao, W. Zhang, P. Ren, X. Han, U. Müller, B. Yilmaz, M. Feyen, H. Gies, F.-S. Xiao, D. De Vos, T. Tatsumi, X. Bao, *Chem. Mater.* **2013**, *25*, 840-847.

[9] S. Maheshwari, E. Jordan, S. Kumar, F. S. Bates, R. L. Penn, D. F. Shantz, M. Tsapatsis, *J. Am. Chem. Soc.* **2008**, *130*, 1507-1516.

[10] L. Jiao, J. R. Regalbuto, *J. Catal.* **2008**, *260*, 329-341.

[11] M. M. J. Treacy, J. B. Higgins, in *Collection of Simulated XRD Powder Patterns for Zeolites (Fifth Edition)*, Elsevier Science B.V., Amsterdam, **2007**, pp. 180-181.

[12] T. G. Appleton, A. J. Bailey, D. R. Bedgood, J. R. Hall, *Inorg. Chem.* **1994**, *33*, 217-226.

[13] E. L. First, C. E. Gounaris, J. Wei, C. A. Floudas, *Phys. Chem. Chem. Phys.* **2011**, *13*, 17339-17358.

[14] G. Prieto, J. Zečević, H. Friedrich, K. P. de Jong, P. E. de Jongh, *Nat Mater* **2013**, *12*, 34-39.

[15] H. N. Aiyer, V. Vijayakrishnan, G. N. Subbanna, C. N. R. Rao, *Surf. Sci.* **1994**, *313*, 392-398.

[16] H. Gies, U. Müller, B. Yilmaz, M. Feyen, T. Tatsumi, H. Imai, H. Zhang, B. Xie, F.-S. Xiao, X. Bao, W. Zhang, T. D. Baerdemaeker, D. De Vos, *Chem. Mater.* **2012**, *24*, 1536-1545.

10.1002/cctc.201800040

Table of Contents

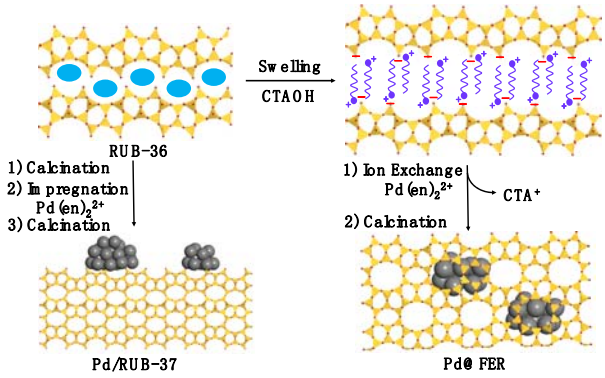

Zhenchao Zhao, Yanlu Li, Mathias Feyen, Robert McGuire, Ulrich Müller, Weiping Zhang**

Pdnanoparticlesencapsulated in FER zeolite through layer reassembling strategy as the shape-selective hydrogenation catalyst

FER zeolite encapsulating Pd nanoparticles with excellent shape-selective catalytic properties were constructed and synthesized through swelling RUB-36, ion exchange, and topotactic conversion processes.